

# Excited-State Mixing in the LOV Domain Proteins: Possible Physics behind the Difference in the Transient Absorption and Transient Stimulated Raman Spectroscopy

Yingliang Liu,\* Aditya S. Chaudhari, Alessandra Picchiotti, Mateusz Rebarz, Miroslav Kloz, Martin Přeček, Jakob Andreasson, and Bohdan Schneider



Cite This: *J. Phys. Chem. Lett.* 2025, 16, 4072–4080



Read Online

ACCESS |



Metrics & More

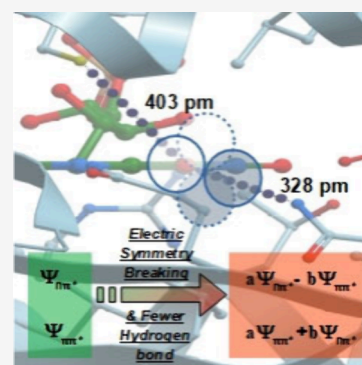


Article Recommendations



Supporting Information

**ABSTRACT:** It remains uncertain whether excited electronic state mixing occurs in the flavin cofactor of the light-oxygen-voltage-sensing (LOV) domain. In this study, we present transient absorption and femtosecond stimulated Raman spectra of both free and EL222 binding flavin mononucleotide (FMN). We observed a change in the shape of the excited-state absorption around 800 nm in the  $S_1$  state transient absorption after binding to EL222, alongside a relative intensity increase of the  $N_1-C_2$  and  $C_2=O_2$  stretching modes in the  $S_1$  state Raman spectra. Based on the previous calculated geometric differences between the  $\pi\pi^*$  and  $n\pi^*$  states, we propose a probable electronic state mixing in EL222 binding FMN. This mixing is favored by the nonsymmetric hydrogen bonding interaction between the flavin  $O_4$  atom and the asparagine residue and fewer hydrogen bonds with the  $O_2$  atom in EL222.



**Introduction.** The light-oxygen voltage-sensing (LOV) domain is a sensor protein that is extensively utilized by various organisms to respond to environmental changes.<sup>1–5</sup> LOV domain proteins typically employ flavin mononucleotide (FMN) as the light receptor. Upon exposure to blue light, the flavin cofactor becomes excited and reacts with a conserved cysteine residue in the LOV domain binding pocket, forming a covalent bond between the cysteine sulfur atom and the  $C_{4a}$  atom of the flavin ring. This adduct formation triggers a rearrangement of the hydrogen bonding network, resulting in an allosteric variation of the protein and transmission of the signal. The light-adapted LOV domain can be thermally activated, leading to the dissociation of the CS bond, within a time frame ranging from seconds to hours depending on the binding pocket structure.<sup>6,7</sup>

Numerous time-resolved studies have investigated the dynamics of the LOV domain proteins. Researchers have utilized transient UV–vis absorption<sup>8–12</sup> and electron paramagnetic resonance spectroscopy<sup>13,14</sup> to monitor changes in the electronic states involved in the primary reaction of the LOV domain. Concurrently, extensive time-resolved infrared spectroscopy studies<sup>15–21</sup> have been conducted to track the corresponding structural dynamics of the primary reactions, hydrogen bond rearrangements, helix unfolding, and signal output domain detachment. Additionally, many theoretical simulations have been performed to examine the electronic structure of the flavin cofactor and the photoinduced reaction mechanism of the LOV domain protein.<sup>22–29</sup>

Through experimentation, it has been discovered that the photoinduced adduction reaction in most LOV domain proteins occurs in the triplet state rather than in the spin-allowed  $S_1$  state. This is different from the reaction mechanism in the BLUF domain (blue light sensors utilizing flavin adenine dinucleotide), where hydrogen transfer takes place in the  $S_1$  state.<sup>30–34</sup> A sole exception to the canonical mechanism was identified in 2016 when Zhu et al. utilized the kinetic isotope effect and found a direct photoinduced adduct channel in the singlet state of CrLOV2 derived from *Chlamydomonas*.<sup>12</sup> However, when CrLOV2 is tagged with 15 positively charged histidine amino acids by its N terminal, it follows the canonical pathway.<sup>35</sup> This experimental evidence suggests that the photochemistry of the LOV domain is highly sensitive to the charge distribution surrounding the protein.

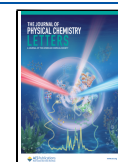
For the unusual behavior of the primary reaction on a spin-forbidden state, Quantum Mechanics/Molecular Mechanics (QM/MM) simulations have demonstrated that the hydrogen transfer barrier in YtvA LOV protein is lower in the  $T_1$  state (5.2 kcal/mol) compared to the  $S_1$  state (9.7 kcal/mol).<sup>22</sup> It remains unclear whether there exist other mechanisms that

**Received:** October 14, 2024

**Revised:** February 17, 2025

**Accepted:** February 17, 2025

**Published:** April 16, 2025



could tune the reaction barrier, aside from the stronger hydrogen-bonding basicity in the  $T_1$  state.

It has been proposed that the mixing of electronic states could alter the potential energy surface (PES). In 2017, Manathunga et al. found that the mixing of the first two excited states in retinal affects the isomerization process of the cofactor.<sup>36,37</sup> Elsaesser's team recently substantiated this through ultrafast terahertz-Stark spectroscopy, noting the significant difference in the electric dipole moments of the  $S_1$  and  $S_2$  states of retinal in bacteriorhodopsin.<sup>38</sup> Additionally, it has been suggested that the mixing between the locally excited state and the charge transfer state contributes to the large Stark tuning rate of the green fluorescent protein chromophore, thereby enhancing its photoacidity.<sup>39</sup>

The question emerges as to whether mixing of excited states also occurs in the LOV domain proteins. It has been discovered that a dark  $n\pi^*$  state exists near the lowest singlet  $\pi\pi^*$  state in flavin.<sup>27</sup> The energy difference between them in the gas phase is estimated to be small, only in the range of tens of meV. However, the coupling is zero unless there is symmetry breaking. The question then is how and to what extent the LOV domains influence the mixing between these two electronic states of flavin.

Resonance Raman spectroscopy is a powerful tool for selectively investigating the structural dynamics of a photo-receptor.<sup>40</sup> Utilizing time-dependent Raman theory,<sup>41–45</sup> the Huang–Rhys factors of Raman transition can be determined from the intensity of the Raman bands. These factors measure the displacement amplitude between the minima of two potential energy surfaces. In 2008, Martias et al. determined the Huang–Rhys factors in rhodamine 6G using femtosecond stimulated Raman spectroscopy (FSRS).<sup>46</sup> More recently, two-dimensional impulsively stimulated resonant Raman spectroscopy has been employed to map the excited-state PES of the chromophore in wild-type green fluorescent protein.<sup>47</sup> Nevertheless, there is a scarcity of FSRS studies on flavin<sup>48,49</sup> and flavin protein.<sup>50,51</sup>

In this study, using the EL222 protein as an example, we aim to understand how the protein binding of the LOV domain affects the electronic structure of the flavin chromophore. Our investigation concentrates on three main aspects: (a) the possibility of mixing between the lowest excited electronic states within the LOV domain protein, (b) its possible impact on the PES and the Raman spectroscopy, and (c) the possible structural origin of the observation.

**Experiments.** The structure of the EL222 protein is shown in Figure 1. This protein comprises one LOV domain and one DNA-binding domain. Details of the experiment and sample preparation have been described previously.<sup>52</sup> Both FMN and EL222 were prepared in a 50 mM MES buffer with 100 mM NaCl at pH = 6.8.

The femtosecond stimulated Raman spectroscopy setup utilized the spectral watermark method.<sup>53</sup> In the current experiment, we employed two independent 1 kHz chirped pulse amplifiers (CPAs), both seeded with 20 fs pulses from a single Ti: sapphire oscillator. One 1.0  $\mu$ J, 475 nm fs pulse beam from one TOPAS served as the actinic pump to initiate the photochemical reaction. Simultaneously, a home-built pulse shaper generates a 5  $\mu$ J, 800 nm picosecond pulse used as the Raman pump, which closely resonates with the excited-state absorption of the  $S_1$  and  $T_1$  states of the flavin cofactor. The probe beam was a supercontinuum generated by focusing a

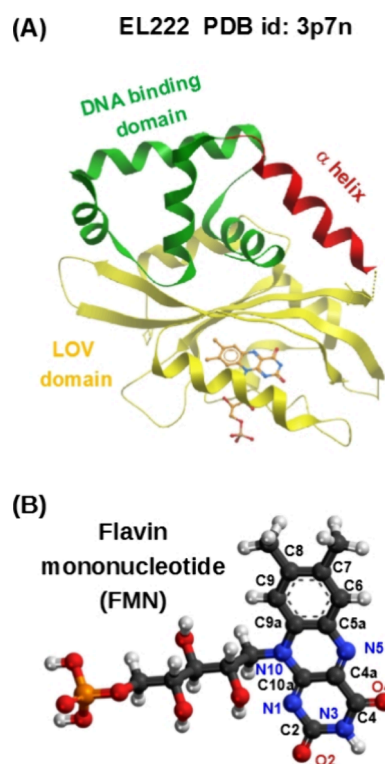


**Figure 1.** Crystal structure of EL222 (A) and chemical structure of its cofactor (B). The LOV domain is displayed in gold, the DNA binding domain in green, and the joint  $\alpha$  helix in red.

1400 nm femtosecond pulse from a second TOPAS onto a moving  $\text{CaF}_2$  plate with a 1 mm thickness.

**Results.** *Evolution of Transient Spectra of the Free FMN and EL222.* The transient absorption spectra for both free FMN and EL222 are plotted in Figures 2A and 2C, respectively. In these two plots, the time delay is illustrated with a rainbow gradient from dark red to purple.

In examining the evolution of the transient spectra in Figure 2A, we observe three major species involved in the light-induced reaction of free FMN. Based on the previous study,<sup>8,54</sup> these species are identified as  $S_1$ ,  $T_1$ , and FMN radical semiquinone. Notably, there are two significant differences in the transient absorption spectra of the  $S_1$  state and the  $T_1$  state: (1) the absence of the excited-state emission (ESE) band between 500 and 600 nm in the  $T_1$  state and (2) a blue shift in the excited-state absorption (ESA) band after intersystem crossing, moving from 800 to 700 nm.

In the transient absorption of EL222, as depicted in Figure 2C, three distinct spectral groups of spectra are evident, corresponding to the  $S_1$ ,  $T_1$  state, and the adduct product. Unlike the situation with free FMN, a notable difference in the relative intensity of the transient absorption is observed in the  $S_1$  and  $T_1$  states. Specifically, the excited-state absorption in the  $T_1$  state of EL222 exhibits a relatively greater intensity compared to that in free FMN.

In Figure 2B,D, the FSRS data are plotted, displaying the spectra with the Stokes shift range between 800 and 1800  $\text{cm}^{-1}$ . The current experiment primarily focuses on the FSRS of the  $S_1$  state and the  $T_1$  state. This is because the electronic transitions of the other transient species are not in resonance with the 800 nm Raman pump.

When intersystem crossing (ISC) occurs from the  $S_1$  to the  $T_1$  states, several changes are observed in the FSRS of both

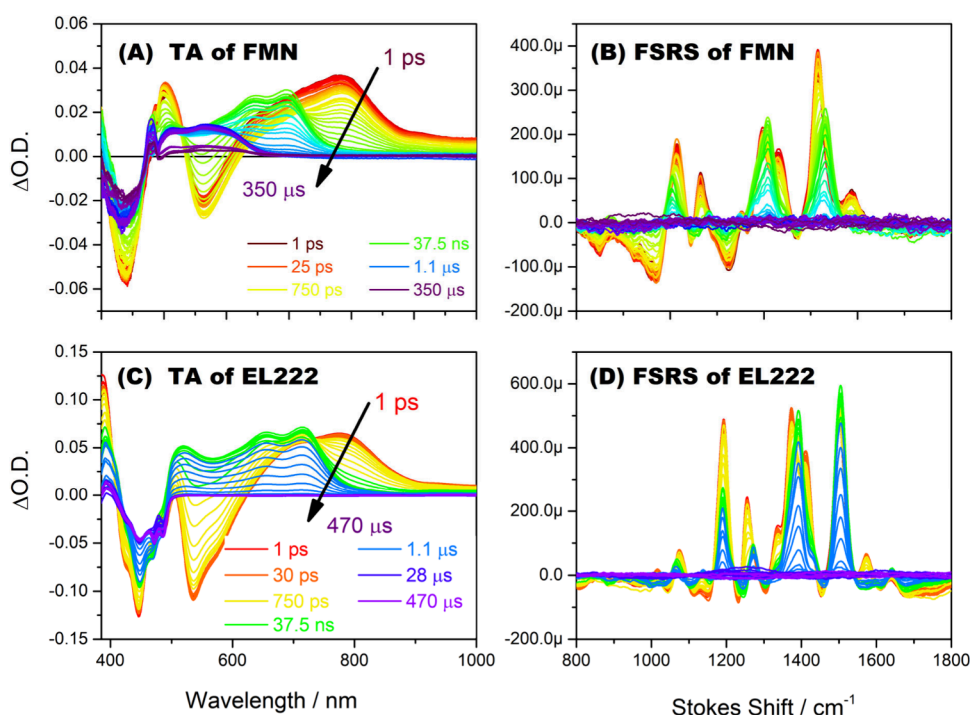


**Figure 2.** Evolution of the transient absorption spectra (A and C) and FSRS spectra (B and D) of the free FMN (top) and EL222 protein (below) with the time delay showing in rainbow color gradient from dark red to purple.

FMN and EL222: (1) the Raman peak at  $1570\text{ cm}^{-1}$  disappears; (2) in the  $1400\text{ cm}^{-1}$  region, three closely spaced peaks in the  $S_1$  state merge into a single peak in the  $T_1$  state; and (3) the  $1250\text{ cm}^{-1}$  peak undergoes a blue shift.

In addition to the similarities, there are two significant differences: (1) the free FMN exhibits a more pronounced  $S_1$ - $T_1$  shift for the  $1500\text{ cm}^{-1}$  peak compared to EL222; (2) the intensity profile of the  $S_1$  state Raman bands in free FMN is quite different from that of the EL222.

*Evolution-Associated Transient Absorption Spectra of Free FMN and EL222.* To understand the spectra, we conducted a global analysis employing the Glotaran program<sup>55</sup> with a sequential model on the experimental transient absorption data. This process yielded the evolution-associated spectra (EAS) and their corresponding time constants shown in the Supporting Information. For the free FMN transient absorption data, five components were necessary to achieve a proper fit, whereas for EL222, only three components were required.

Here, we present selected evolution-associated transient absorption spectroscopy of FMN in two distinct chemical environments. In Figure 3A, the black curve illustrates the EASs of the fully equilibrated  $S_1$  state of free FMN in water with a lifetime of 3.3 ns; meanwhile, the red curve represents the  $S_1$  state of FMN within the EL222 protein exhibiting a lifetime of 2.6 ns. Notable differences are evident in the excited-state absorption band for wavelengths exceeding 600 nm. Specifically, the excited-state absorption band of FMN in the EL222 protein differs in shape compared to that of free FMN. First, it features a shoulder centered around 700 nm. Second, the excited-state absorption band displays a wider bandwidth compared to the free FMN. In Table 1, we list the peak positions of this excited-state absorption band and its width at  $1/e$  of the maximum height.

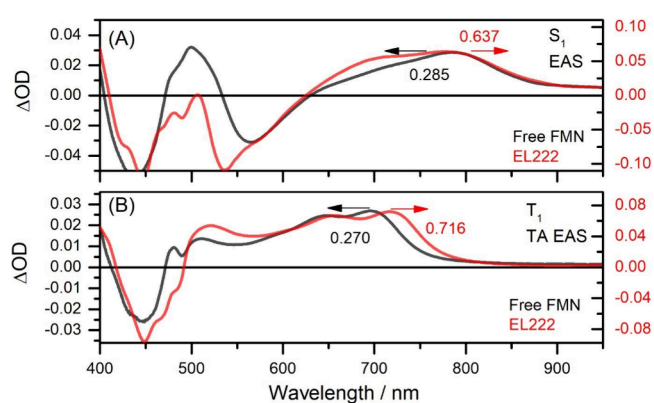


**Figure 3.** Comparison of the evolution-associated transient absorption spectra of the free FMN (A) on the top and EL222 protein (B) on the bottom.

**Table 1.** List of global fitting components and peak width of the transient absorption resonance with the 800 nm Raman pump

Species	Global fitting component	Physical origin	The peak position of the band that resonance with 800 nm Raman pump	Position at Height/e	Width in $\text{cm}^{-1}$ @ Height/e
FMN	EAS3	$S_1$	788	867	2230
	EAS4	$T_1$	695	747	1990
EL222	EAS1	$S_1$	777	869	2720
	EAS2	$T_1$	717	764	1710

Figure 3B illustrates the  $T_1$  state EASs of free FMN, which has a lifetime of  $0.57\text{ }\mu\text{s}$ , and its EL222-binding state, with a lifetime of  $0.65\text{ }\mu\text{s}$ . There is no significant structural alteration in the  $T_1$  state absorption bands between 600 and 800 nm.

Upon binding, the main change is a red shift in the  $T_1$  state absorption bands.

In addition to noting variations in the bandwidth, in Figure 3, we recorded the height of the excited-state absorption bands mentioned above. For free FMN, the reddest peak of the  $T_1$  state appears lower than that of the fully equilibrated  $S_1$  state, 0.270 compared to 0.285. Conversely, in the case of EL222, the  $T_1$  state exhibits a greater height than the  $S_1$  state (measuring 0.716 versus 0.637). This indicates a 16% decrease of the relative height of the excited-state absorption band, when FMN is present in EL222. In previous studies, it has been demonstrated that the LOV domain shares a comparable  $S_1$ - $T_1$  intersystem crossing (ISC) quantum yield  $\Phi_T$  of 0.6 with free FMN<sup>1,8,56–58</sup> and that the LOV cavity has little effect on  $\Phi_T$ ,<sup>1</sup> suggesting a different origination for the current observation.

*Evolution-Associated Excited-State Resonance Raman Spectra of Free FMN and EL222.* The changes in the chromophore structure and its interaction with the environment in the excited states were also monitored using FSRs across the spectral range of 100 to 1800  $\text{cm}^{-1}$ .

To distinguish the Raman signatures of various species, we also conducted a global analysis of the FSRs data using a sequential model. We removed the baseline of the EASs from the global fit to ensure that all resonant Raman bands are positive, with the procedure detailed in the Supporting Information.

In the free FMN, the first three Raman EASs come from their  $S_1$  state with different solvation structures and the fourth component to the  $T_1$  state. However, the EL222 FSRs experimental data yielded only one  $S_1$  Raman spectrum and one  $T_1$  Raman spectrum. Here, we have chosen the fully equilibrated  $S_1$  state Raman and  $T_1$  state Raman with Stokes shift between 800 and 1800  $\text{cm}^{-1}$  and presented them in Figure 4.

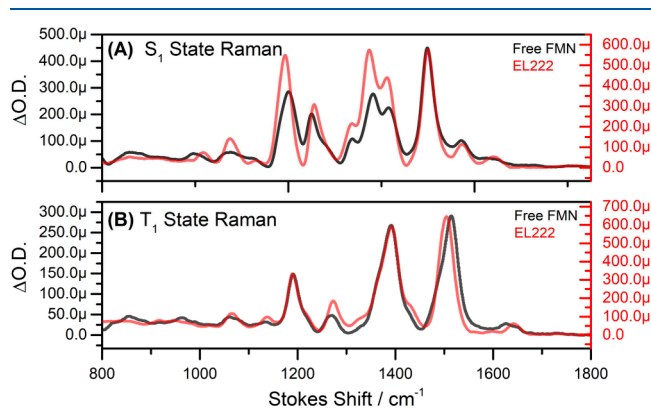


**Figure 4.** Comparison of evolution-associated FSRs spectra of the free FMN (A) (on the top) and EL222 protein (B) (in the below) with Stokes shift between 800  $\text{cm}^{-1}$  to 1800  $\text{cm}^{-1}$ .

In this work, we use the assignment of Weigel<sup>48</sup> and Iuliano.<sup>50,59</sup> We classify the normal modes into two groups: the C=O stretching modes above 1600  $\text{cm}^{-1}$ ; ring breathing modes involved the stretching of the C–C and C–N bonds in the flavin ring from 1000 to 1600  $\text{cm}^{-1}$ .

*The C=O Stretching Modes above 1600  $\text{cm}^{-1}$ .* In this region, the Raman spectra exhibit only one weak band in both the  $S_1$  and  $T_1$  states. For the  $S_1$  state, the C=O stretching vibrations are observed above 1600  $\text{cm}^{-1}$  and peak at 1634  $\text{cm}^{-1}$  for free

FMN and 1640  $\text{cm}^{-1}$  for EL222 binding FMN. In contrast, the  $T_1$  state Raman spectra show the C=O stretching vibration band peaking at 1633  $\text{cm}^{-1}$  for free FMN and 1643  $\text{cm}^{-1}$  for EL222. This blue shift in the EL222 binding FMN suggests a weaker hydrogen bonding interaction within the binding pocket compared with that free FMN in water. Aside from the blue shift, there is also a notable increase in the Raman intensity of the C=O stretching mode in the  $S_1$  state after EL222 binding.

*The Ring Stretching Modes between 1000 and 1600  $\text{cm}^{-1}$ .* The  $S_1$  State Raman. In both scenarios, the 1500  $\text{cm}^{-1}$  Raman band consistently ranks among the most prominent bands. This band from the  $S_1$  state has a contribution from  $C_{5a}$ – $C_{9a}$  stretching modes. It also incorporates other local modes, such as  $N_1$ – $C_{10A}$  stretching mode, which is shared with the 1572  $\text{cm}^{-1}$  normal modes.<sup>48,50,59</sup>

In the  $S_1$  state Raman spectra, three ring-breathing normal modes have contributions from the  $N_1$ – $C_2$  stretching mode. These modes have peaks at 1416 (1412), 1383 (1374), and 1200 (1193)  $\text{cm}^{-1}$  for free FMN (EL222 binding FMN), respectively. Upon protein binding, all of these modes display a red shift. Additionally, their relative intensity increases significantly compared to the 1500  $\text{cm}^{-1}$  band. A similar  $S_1$  state Raman feature was also observed in the case of AsLOV2 by Iuliano et al. in 2020<sup>50,59</sup> and BLUF by Hontani et al. in 2023.<sup>51</sup>

*The  $T_1$  State Raman.* When it comes to the  $T_1$  state Raman spectra, there is a distinct contrast from the  $S_1$  state Raman spectrum within the same region. First, unlike the  $S_1$  state, the relative band intensity remains largely unchanged when the FMN is incorporated into the EL222 binding pocket. This behavior closely resembles that of the corresponding transient absorption in the  $T_1$  state. Second, the 1500  $\text{cm}^{-1}$  band in the  $S_1$  state Raman spectra exhibits a blue shift as the FMN does an ISC from the  $S_1$  state to the  $T_1$  state. This phenomenon is observed in both the free and EL222 binding cases, with the only difference in the magnitude of the shift: +5  $\text{cm}^{-1}$  for EL222 and +17  $\text{cm}^{-1}$  for free FMN. Third, within the frequency range of 1300 to 1450  $\text{cm}^{-1}$ , there is only one predominating band in the  $T_1$  state Raman spectra, peaking at 1391  $\text{cm}^{-1}$  for free FMN and 1392  $\text{cm}^{-1}$  for EL222.

**Discussions.** *Stimulated Raman Intensity and Displacement between Potential Energy Surface Minima.* In the FSRs experiment, we measure the imaginary part of the third-order susceptibility of matter  $\text{Im}\{\chi_{\text{SRS}}^{(3)}\}$ .<sup>60</sup>

$$\chi_{\text{SRS}}^{(3)} \propto \frac{\langle g_0 | M | e_0 \rangle^4}{\omega_{\text{vib}} - (\omega_{\text{pump}} - \omega_{\text{stokes}}) - i\Gamma_{\text{vib}}} \times \left( \sum_{\nu} \frac{\langle 0 | \nu \rangle \langle \nu | 1 \rangle}{\omega_{g_0, \nu} - \omega_{\text{pump}} - i\Gamma_{\nu}} \right)^2 \quad (1)$$

In the equation presented above,  $\langle g_0 | M | e_0 \rangle$  represents the electronic transition moment;  $\omega_{\text{stokes}}$  denotes the Stokes frequency. The symbol  $\Gamma_{\text{vib}}$  indicates the line width of the vibrational transition, and  $\omega_{g_0, \nu}$  stands for the vibration resolved electronic transition frequency; the letters  $g$  and  $e$  refer to the ground and excited electronic states. The symbols  $|0\rangle$ ,  $|1\rangle$ , and  $|\nu\rangle$  signify the ground, the first, and the intermediate vibronic states involved in the Raman transition. The integral  $\langle 0 | \nu \rangle \langle \nu | 1 \rangle$  is a function of the dimensionless shift  $\Delta_{e,Q}$  between the ground-state PES minimum and the excited-

state PES minimum along the normal mode coordinate  $Q$ . The factor  $\left(\sum_{\nu} \frac{1}{\omega_{g_0, ev} - \omega_{pump} - i\Gamma_{ev}}\right)^2$  accounts for the off-resonance correction.

The factor  $\frac{1}{\omega_{vib} - (\omega_{pump} - \omega_{stokes}) - i\Gamma_{vib}}$  determines the Raman spectral profile including an imaginary part, denoted as  $\frac{\Gamma_c}{\Delta\omega^2 + \Gamma_c^2}$ , where  $\Delta\omega = \omega_{vib} - (\omega_{pump} - \omega_{stokes})$  represents the deviation from central frequency of the Raman transition. The integral of  $\frac{\Gamma_c}{\Delta\omega^2 + \Gamma_c^2}$  is a constant, suggesting that the factor  $\frac{1}{\omega_{vib} - (\omega_{pump} - \omega_{stokes}) - i\Gamma_{vib}}$  does not affect the Raman peak area but solely the Raman line shape. The equation described above can be further simplified into the following form.

$$\chi_{SRS}^{(3)} \propto \frac{\langle g_0 | M | e_0 \rangle^4}{\Delta\omega - i\Gamma_{vib}} \times \left( \sum_{\nu} \frac{\langle 0|v\rangle\langle v|1\rangle}{\omega_{g_0, ev} - \omega_{pump} - i\Gamma_{ev}} \right)^2 \quad (2)$$

If the displacement  $\Delta_{e,Q}$  is small, primarily the  $e_0$  and  $e_1$  states contribute to the Raman transition.<sup>61–64</sup> Since the integrations  $\langle 0|0\rangle\langle 0|1\rangle$  and  $\langle 0|1\rangle\langle 1|1\rangle$  are linear with  $\Delta_{e,Q}$ .

$$\langle 0|1\rangle\langle 1|1\rangle \approx -\langle 0|0\rangle\langle 0|1\rangle \approx -\frac{\Delta_e}{2} \quad (3)$$

Therefore, the above equation can be further simplified.<sup>62</sup>

$$\chi_{SRS}^{(3)} \propto \frac{\langle g_0 | M | e_0 \rangle^4}{\Delta\omega - i\Gamma_{vib}} (\Delta_{e,Q})^2 \left( \frac{1}{\omega_{e_0} - \omega_{pump} - i\Gamma_{e_0}} - \frac{1}{\omega_{e_1} - \omega_{pump} - i\Gamma_{e_1}} \right)^2 \quad (4)$$

From this equation, it is evident that the FSRS signal of a particular vibrational mode is proportional to the square of its corresponding displacement  $\Delta_{e,Q}$ . Using this relation, we can extract information about the relative displacement amplitude at the excited-state PES minima from the area of the Raman bands. Specifically, from the current Raman data, there is a relative increase in the displacement of all  $N_1-C_2$  and  $C_2=O_2$  stretching modes compared to those of the other stretching modes.

Assuming the bandwidth of the electronic transition spectra primarily arises from the Franck–Condon effect, the absolute displacement amplitude can be estimated from the width of the corresponding UV–vis absorption band using the following equation.<sup>44,65</sup>

$$W_{@(\text{Height}/e)} = 2 \left[ \sum_Q (\Delta_{e,Q}^2 \nu_Q^2) \right]^{1/2} \quad (5)$$

Here,  $W_{@(\text{Height}/e)}$  is the full width at the  $1/e$  maximum of the absorption band. In this scenario, we disregard the influence of solvation. This equation indicates that the bandwidth of the transient absorption is proportional to the square root of the total fundamental Raman intensity. Since the C–H and N–H stretching modes do not participate in the stretching of the  $\pi$  bonds, their enhancement is minimal.<sup>66–68</sup>

Table 1 presents the peak positions of the transient absorption bands that resonate with 800 nm, along with their width measured at  $1/e$  of the height. The bandwidth of

the EL222 binding  $S_1$  state is  $2720 \text{ cm}^{-1}$ , which is over 22% broader than that of the equilibrated free FMN, recorded at  $2230 \text{ cm}^{-1}$ . This broadening indicates a greater overall displacement in the PES minima. In contrast, for the  $T_1$  state absorption, the bandwidth is  $1990 \text{ cm}^{-1}$  for the free FMN, and it is  $1710 \text{ cm}^{-1}$  for EL222. The narrowing of the  $T_1$  state absorption bands can be attributed to the homogeneous chemical environment in the EL222 binding pocket. In contrast to the  $T_1$  state, there must be other mechanisms responsible for the broadening observed in the  $S_1$  state absorption of EL222, for instance, the increasing in overall displacement with contribution from the  $N_1-C_2$  and  $C_2=O_2$  stretching modes. In the Supporting Information, employing the nonresonant spontaneous Raman theory, we disclose a similar increase in the displacement of the  $N_1-C_2$  and  $C_2=O_2$  stretching modes.

*Variation in the Topology of the  $S_1$  State Potential Energy Surface and the Electronic-State Mixing.* For the stretching modes, variation in displacement between PES minima indicates changes in the corresponding bond lengths. To understand the origin of the  $N_1-C_2$  bond length variation, we refer to previous quantum calculations, focusing on the geometry of the low-lying excited states, i.e., the  $S_1$  and  $S_2$  states. Salzmann et al. demonstrated that the most significant change occurs in the length of the  $N_1-C_2$  and  $C_2=O_2$  bond lengths as flavin transitions from the  $\pi\pi^*$  state to the  $n\pi^*$  state: the  $N_1-C_2$  bond contracts by 9 pm and  $C_2=O_2$  bond extends by 9 pm, while all the other bonds exhibit changes of no more than 2 pm.<sup>27</sup> As a result, the possible mixing of these two electronic states results in a more substantial alteration in the  $N_1-C_2$  and  $C_2=O_2$  bond length than the other bonds, causing a more profound increase in the displacement and intensity of the corresponding Raman peaks.

In addition to altering the positions of the nuclei, state mixing also modifies the curvature of the related PES.<sup>69</sup> The redshift observed in the normal modes involving the  $N_1-C_2$  stretching mode reflects a decrease in the corresponding force constant of the lower PES following the excited-state mixing.

$$k_{E_{\pm}}(0) = k_0 \left\{ 1 \mp \frac{4k_0 b^2 \beta^2}{\left[ \left( \frac{1}{2} k_0 b^2 + \Delta E \right)^2 + 4\beta^2 \right]^{3/2}} \right\} \quad (6)$$

Here,  $k_0$  is the force constant of the parabolic potential curve prior to mixing,  $b$  is the displacement between the minima of the PESs, and  $\Delta E$  is the energy difference between the minima of the PESs. Additionally,  $\beta$  represents the coupling constant.  $k_{E_{\pm}}$  is the force constant after the electronic state mixing.

In addition to affecting transient absorption and vibrational Raman spectroscopy, the electronic state mixing between  $\pi\pi^*$  and  $n\pi^*$  states also activates the dark  $n\pi^*$  state in electric dipole transitions. An electronic Raman transition may take place between the new  $S_{1*}$  state and the  $S_{2*}$  state after mixing. This Raman transition between electronic states may contribute to an unavoidable Raman background when employing the spectral watermark method. This broad electronic Raman transition contributes to the background in vibrational Raman spectroscopy. It can only be removed by implementing a time domain Raman technique similar to the field-resolved infrared spectroscopy developed by Krausz et al.<sup>70</sup>

*Structural Reasons for the Excited-State Mixing in the LOV Domain.* Quantum-state mixing depends on the coupling  $\beta$  and the energy gap  $\Delta E$  between them. In isolated flavin, the nonbonding orbitals of nitrogen and oxygen are symmetric with respect to the flavin plane, belonging to the total symmetric representation  $A'$ , and the  $\pi$  orbital antisymmetric about the plane, placing it in the  $A''$  representation. These two orbitals are orthogonal to each other, vanishing the orbital overlap and state coupling. This is true if the nuclei are frozen on the plane and disregarding the out-of-plane bending induced mechanical symmetry breaking. More is different.<sup>71</sup> Solvation and protein binding can disrupt the  $C_s$  symmetry of the electric field surrounding the cofactor via the intermolecular interactions. More specifically, the hydrogen bonding interaction between the amino acid residues and the flavin ring breaks the symmetry of the electric field around the cofactor. As shown in Figure 5, one significant contribution to the

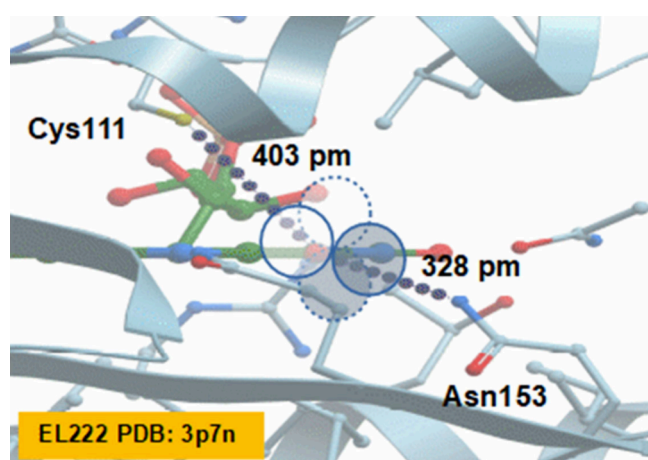


**Figure 5.** Hydrogen bond acceptor atoms and their atomic orbitals involved in the electrical symmetry breaking and state mixing of the  $n\pi^*$  and  $\pi\pi^*$  states. The  $p_z$  orbitals of the O4 atom are shown in a dashed circle, while the corresponding  $sp^2$  orbitals are in a solid circle. They are parts of the  $\pi$  HOMO orbital and the nonbonding HOMO–1 orbital, respectively. The phase of the atomic orbital in HOMO and HOMO–1 is shown as a different color.

orbital overlapping arises from the hydrogen bond with the asparagine residue Asn153. The Asn153 forms a hydrogen bond with O<sub>4</sub> through its NH<sub>2</sub> group with a distance  $d(N-O_4)$  of 328 pm. The N atom of Asn153 is positioned approximately 140 pm below the flavin plane. Meanwhile, there is also one cysteine residue Cys111 in the quite opposite position of Asn153, with its –SH group above the plane, forming a weak SH...O<sub>4</sub> hydrogen bond at a distance  $d(S-O_4)$  of 403 pm.

Similar hydrogen bond interactions occur in other LOV proteins: Asn89 of YtvA (PDB ID:2PR5),<sup>72</sup> Asn90 of AsLOV2 (PDB ID:2 V1A),<sup>73</sup> Asn101 of AsLOV2 (PDB ID:4WF0),<sup>74</sup> Asn87 of AtLOV2 (PDB ID:4EEP),<sup>75</sup> Asn83 of CrLOV1 (PDB ID:1N9L),<sup>76</sup> Asn98 of RsLOV (PDB ID:4HJ4),<sup>77</sup> Asn125 of VVD (PDB ID:3RH8),<sup>78</sup> and Asn326 of PAL (PDB ID:6HMJ).<sup>79</sup> This Asn residue is conserved in the LOV domain. Compared to the fluctuating and probably more symmetric hydrogen bonding interaction with water for free FMN, this stable asymmetric hydrogen bonding in the LOV domain binding pocket provides a constant and stronger coupling between the  $\pi\pi^*$  state and the  $n\pi^*$  states.

In addition to the static electric symmetry breaking by the hydrogen bonding interaction, the energy gap between the  $n\pi^*$  and  $\pi\pi^*$  states also narrows compared to the free FMN case. Our Raman spectra showed a 6 cm<sup>-1</sup> blue shift of the S<sub>1</sub> state C=O stretching modes when FMN binds to EL222, suggesting weak or fewer hydrogen bonding interactions between the flavin ring and the binding pocket compared to water. This is consistent with the long distance between the C=O group and the threonine T88 residue in the crystal structure, with  $d(O_{T88}-N_1)$  of 581 pm and  $d(O_{T88}-O_2)$  of 489 pm, indicating fewer hydrogen bonds between the cofactor FMN and its chemical environment. Due to the attractive interaction of the nonbonding electron with the positively charged hydrogen, the hydrogen bonding interaction stabilizes the nonbonding state, hence enlarging the bandgap between the nonbonding orbital and the lowest unoccupied  $\pi_L$  orbital.<sup>80</sup> On the contrary, the fewer hydrogen bonds will decrease the energy gap between the nonbonding orbital and the  $\pi_L$  orbital and narrow the gap between the  $n\pi^*$  and  $\pi\pi^*$  states.

The analysis indicates that the EL222 binding with the FMN cofactor results in a greater coupling and a narrower energy gap compared to those of free FMN. Both factors enhance the quantum mixing between these two electronic states, contributing to variations observed in the S<sub>1</sub> state transient absorption and FSRS spectra.

**Conclusions.** We have performed a comparative analysis of femtosecond stimulated Raman spectroscopy of free flavin in water and its binding state in EL222. Our analysis suggests a mixing of the dark  $n\pi^*$  state (S<sub>2</sub>) into the  $\pi\pi^*$  state (S<sub>1</sub>) in the LOV domain protein EL222. This state mixing manifests in two spectroscopic features. First, a reshaping of the transition absorption from the S<sub>1</sub> state. Second, the mixing of these two states modifies the topology of the S<sub>1</sub> potential energy surface, especially in the length of N<sub>1</sub>–C<sub>2</sub> and C<sub>2</sub>=O<sub>2</sub> bonds; hence the Stokes shift and Raman intensity of the corresponding stretching modes. Two structural reasons contribute to the effective electronic state mixing in EL222. Effective and constant coupling arises from the asymmetric hydrogen bonding interaction with the nonbonding flavin orbital in the binding pocket. Simultaneously, the narrow energy gap comes from the fewer hydrogen bond interactions and the decrease in the  $n\pi^*$  state energy.

## ■ ASSOCIATED CONTENT

### Supporting Information

The Supporting Information is available free of charge at <https://pubs.acs.org/doi/10.1021/acs.jpcllett.4c02978>.

- (1) UV–vis absorption of the samples;
  - (2) Evolution-associated spectroscopy and baseline correction of the EAS Raman spectroscopy;
  - (3) Assignment of the vibrational modes;
  - (4) Displacement obtained using the off-resonance spontaneous Raman intensity frame;
  - (5) Other effects on the Raman spectroscopy (PDF)
- Transparent Peer Review report available (PDF)

## ■ AUTHOR INFORMATION

### Corresponding Author

Yingliang Liu – Institute of Biotechnology of the Czech Academy of Sciences, BIOCEV, CZ-252 50 Vestec, Czechia; The Extreme Light Infrastructure ERIC, ELI Beamlines Facility, CZ-252 41 Dolní Břežany, Czech Republic; Weihai Kingfull Electronics Co., Ltd., CN-264204 Weihai, China;

orcid.org/0000-0002-4089-688X; Email: liuyl.sino@gmail.com

## Authors

**Aditya S. Chaudhari** – Institute of Biotechnology of the Czech Academy of Sciences, BIOCEV, CZ-252 50 Vestec, Czechia

**Alessandra Picchiotti** – The Extreme Light infrastructure ERIC, ELI Beamlines Facility, CZ-252 41 Dolní Břežany, Czech Republic; Institute for Nanostructure and Solid State Physics, University of Hamburg, DE-22761 Hamburg, Germany

**Mateusz Rebarz** – The Extreme Light infrastructure ERIC, ELI Beamlines Facility, CZ-252 41 Dolní Břežany, Czech Republic

**Miroslav Kloz** – The Extreme Light infrastructure ERIC, ELI Beamlines Facility, CZ-252 41 Dolní Břežany, Czech Republic

**Martin Přeček** – The Extreme Light infrastructure ERIC, ELI Beamlines Facility, CZ-252 41 Dolní Břežany, Czech Republic

**Jakob Andreasson** – The Extreme Light infrastructure ERIC, ELI Beamlines Facility, CZ-252 41 Dolní Břežany, Czech Republic

**Bohdan Schneider** – Institute of Biotechnology of the Czech Academy of Sciences, BIOCEV, CZ-252 50 Vestec, Czechia

Complete contact information is available at:

<https://pubs.acs.org/10.1021/acs.jpcllett.4c02978>

## Notes

The authors declare no competing financial interest.

## ACKNOWLEDGMENTS

The work was supported by the project ADONIS (CZ.02.1.01/0.0/0.0/16\_019/0000789) and ELIBIO (CZ.02.1.01/0.0/0.0/15\_003/0000447) from the European Regional Development Fund and the Ministry of Education, Youth and Sports (MEYS) of the Czech Republic. Yingliang Liu thanks Dr. Jakub Dostál from ELI Beamlines for discussions.

## REFERENCES

- (1) Losi, A. Invited Review Flavin-Based Blue-Light Photosensors: A Photobiophysics Update. *Photochem. Photobiol.* **2007**, *83*, 1283–1300.
- (2) Losi, A.; Gärtner, W. Solving Blue Light Riddles: New Lessons from Flavin-Binding LOV Photoreceptors. *Photochem. Photobiol.* **2017**, *93* (1), 141–158.
- (3) Jansen, V.; Jikeli, J. F.; Wachten, D. How to Control Cyclic Nucleotide Signaling by Light. *Curr. Opin Biotechnol.* **2017**, *48*, 15–20.
- (4) Shcherbakova, D. M.; Shemetov, A. A.; Kaberniuk, A. A.; Verkhusha, V. V. Natural Photoreceptors as a Source of Fluorescent Proteins, Biosensors, and Optogenetic Tools. *Annu. Rev. Biochem.* **2015**, *84* (1), 519–550.
- (5) Repina, N. A.; Rosenbloom, A.; Mukherjee, A.; Schaffer, D. V.; Kane, R. S. At Light Speed: Advances in Optogenetic Systems for Regulating Cell Signaling and Behavior. *Annu. Rev. Chem. Biomol. Eng.* **2017**, *8*, 13–39.
- (6) Zayner, J. P.; Sosnick, T. R. Factors That Control the Chemistry of the LOV Domain Photocycle. *PLoS One* **2014**, *9* (1), No. e87074.
- (7) Zoltowski, B. D.; Vaccaro, B.; Crane, B. R. Mechanism-Based Tuning of a LOV Domain Photoreceptor. *Nat. Chem. Biol.* **2009**, *5* (11), 827–834.
- (8) Kennis, J. T. M.; Crosson, S.; Gauden, M.; van Stokkum, I. H. M.; Moffat, K.; van Grondelle, R. Primary Reactions of the LOV2 Domain of Phototropin, a Plant Blue-Light Photoreceptor. *Biochemistry* **2003**, *42* (12), 3385–3392.
- (9) Kennis, J. T. M.; Van Stokkum, I. H. M.; Crosson, S.; Gauden, M.; Moffat, K.; van Grondelle, R. The LOV2 Domain of Phototropin: A Reversible Photochromic Switch. *J. Am. Chem. Soc.* **2004**, *126* (14), 4512–4513.
- (10) Kutta, R. J.; Magerl, K.; Kensity, U.; Dick, B. A Search for Radical Intermediates in the Photocycle of LOV Domains. *Photochemical & Photobiological Sciences* **2015**, *14* (2), 288–299.
- (11) Bauer, C.; Rabl, C. R.; Heberle, J.; Kottke, T. Indication for a Radical Intermediate Preceding the Signaling State in the LOV Domain Photocycle. *Photochem. Photobiol.* **2011**, *87* (3), 548–553.
- (12) Zhu, J.; Mathes, T.; Hontani, Y.; Alexandre, M. T. A.; Toh, K. C. C.; Hegemann, P.; Kennis, J. T. M. M. Photoadduct Formation from the FMN Singlet Excited State in the LOV2 Domain of *Chlamydomonas Reinhardtii* Phototropin. *J. Phys. Chem. Lett.* **2016**, *7* (21), 4380–4384.
- (13) Schleicher, E.; Kowalczyk, R. M.; Kay, C. W. M.; Hegemann, P.; Bacher, A.; Fischer, M.; Bittl, R.; Richter, G.; Weber, S. On the Reaction Mechanism of Adduct Formation in LOV Domains of the Plant Blue-Light Receptor Phototropin. *J. Am. Chem. Soc.* **2004**, *126* (35), 11067–11076.
- (14) Tsukuno, H.; Ozeki, K.; Kobayashi, I.; Hisatomi, O.; Mino, H. Flavin-Radical Formation in the Light-Oxygen-Voltage-Sensing Domain of the Photozipper Blue-Light Sensor Protein. *J. Phys. Chem. B* **2018**, *122* (38), 8819–8823.
- (15) Pfeifer, A.; Majerus, T.; Zikihara, K.; Matsuoka, D.; Tokutomi, S.; Heberle, J.; Kottke, T. Time-Resolved Fourier Transform Infrared Study on Photoadduct Formation and Secondary Structural Changes within the Phototropin LOV Domain. *Biophys. J.* **2009**, *96* (4), 1462–1470.
- (16) Konold, P. E.; Mathes, T.; Weißenborn, J.; Groot, M. L.; Hegemann, P.; Kennis, J. T. M. Unfolding of the C-Terminal  $\alpha$  Helix in the LOV2 Photoreceptor Domain Observed by Time-Resolved Vibrational Spectroscopy. *J. Phys. Chem. Lett.* **2016**, *7* (17), 3472–3476.
- (17) Alexandre, M. T. A.; Domratcheva, T.; Bonetti, C.; van Wilderen, L. J. G. W.; van Grondelle, R.; Groot, M.-L.; Hellingwerf, K. J.; Kennis, J. T. M. Primary Reactions of the LOV2 Domain of Phototropin Studied with Ultrafast Mid-Infrared Spectroscopy and Quantum Chemistry. *Biophys. J.* **2009**, *97* (1), 227–237.
- (18) Zayner, J. P.; Mathes, T.; Sosnick, T. R.; Kennis, J. T. M. Helical Contributions Mediate Light-Activated Conformational Change in the LOV2 Domain of *Avena Sativa* Phototropin I. *ACS Omega* **2019**, *4* (1), 1238–1243.
- (19) Iuliano, J. N.; Collado, J. T.; Gil, A. A.; Ravindran, P. T.; Lukacs, A.; Shin, S.; Woroniecka, H. A.; Adamczyk, K.; Aramini, J. M.; Edupuganti, U. R.; Hall, C. R.; Greetham, G. M.; Sazanovich, I. V.; Clark, I. P.; Daryae, T.; Toettcher, J. E.; French, J. B.; Gardner, K. H.; Simmerling, C. L.; Meech, S. R.; Tonge, P. J. Unraveling the Mechanism of a LOV Domain Optogenetic Sensor: A Glutamine Lever Induces Unfolding of the  $\alpha$  Helix. *ACS Chem. Biol.* **2020**, *15* (10), 2752–2765.
- (20) Iuliano, J. N.; Gil, A. A.; Laptanok, S. P.; Hall, C. R.; Tolentino Collado, J.; Lukacs, A.; Hag Ahmed, S. A.; Abyad, J.; Daryae, T.; Greetham, G. M.; Sazanovich, I. V.; Illarionov, B.; Bacher, A.; Fischer, M.; Towrie, M.; French, J. B.; Meech, S. R.; Tonge, P. J. Variation in LOV Photoreceptor Activation Dynamics Probed by Time-Resolved Infrared Spectroscopy. *Biochemistry* **2018**, *57* (5), 620–630.
- (21) Gil, A. A.; Laptanok, S. P.; French, J. B.; Iuliano, J. N.; Lukacs, A.; Hall, C. R.; Sazanovich, I. V.; Greetham, G. M.; Bacher, A.; Illarionov, B.; Fischer, M.; Tonge, P. J.; Meech, S. R. Femtosecond to Millisecond Dynamics of Light Induced Allosteric in the *Avena Sativa* LOV Domain. *J. Phys. Chem. B* **2017**, *121* (5), 1010–1019.
- (22) Chang, X.; Gao, Y.; Fang, W.; Cui, G.; Thiel, W. Quantum Mechanics/Molecular Mechanics Study on the Photoreactions of Dark- and Light-Adapted States of a Blue-Light YtvA LOV Photoreceptor. *Angew. Chem., Int. Ed.* **2017**, *56* (32), 9341–9345.
- (23) Nakagawa, S.; Weingart, O.; Marian, C. M. Dual Photochemical Reaction Pathway in Flavin-Based Photoreceptor LOV Domain: A

- Combined Quantum-Mechanics/Molecular-Mechanics Investigation. *J. Phys. Chem. B* **2017**, *121* (41), 9583–9596.
- (24) Domratcheva, T.; Fedorov, R.; Schlichting, I. Analysis of the Primary Photocycle Reactions Occurring in the Light, Oxygen, and Voltage Blue-Light Receptor by Multiconfigurational Quantum-Chemical Methods. *J. Chem. Theory Comput* **2006**, *2* (6), 1565–1574.
- (25) Freddolino, P. L.; Gardner, K. H.; Schulten, K. Signaling Mechanisms of LOV Domains: New Insights from Molecular Dynamics Studies. *Photochemical & Photobiological Sciences* **2013**, *12* (7), 1158–1170.
- (26) Song, S.-H.; Freddolino, P. L.; Nash, A. I.; Carroll, E. C.; Schulten, K.; Gardner, K. H.; Larsen, D. S. Modulating LOV Domain Photodynamics with a Residue Alteration Outside the Chromophore Binding Site. *Biochemistry* **2011**, *50* (13), 2411–2423.
- (27) Salzmans, S.; Tatchen, J.; Marian, C. M. The Photophysics of Flavins: What Makes the Difference between Gas Phase and Aqueous Solution? *J. Photochem. Photobiol. A Chem.* **2008**, *198* (2–3), 221–231.
- (28) Salzmans, S.; Marian, C. M. The Photophysics of Alloxazine: A Quantum Chemical Investigation in Vacuum and Solution. *Photochemical & Photobiological Sciences* **2009**, *8* (12), 1655–1666.
- (29) Salzmans, S.; Silva-Junior, M. R.; Thiel, W.; Marian, C. M. Influence of the LOV Domain on Low-Lying Excited States of Flavin: A Combined Quantum-Mechanics/Molecular-Mechanics Investigation. *J. Phys. Chem. B* **2009**, *113* (47), 15610–15618.
- (30) Nunthaboot, N.; Kido, N.; Tanaka, F.; Lugsanangarm, K.; Nueangaudom, A.; Pianwanit, S.; Kokpol, S. Relationship between Rate of Photoinduced Electron Transfer and Hydrogen Bonding Chain of Tyrosine-Glutamine-Flavin in Flavin Photoreceptors: Global Analyses among Four TePixDs and Three AppAs. *J. Photochem. Photobiol. A Chem.* **2013**, *252*, 14–24.
- (31) Kang, X.; Chen, Z.; Zhou, Z.; Zhou, Y.; Tang, S.; Zhang, Y.; Zhang, T.; Ding, B.; Zhong, D. Direct Observation of Ultrafast Proton Rocking in the BLUF Domain. *Angew. Chem., Int. Ed.* **2022**, *61* (10), 1–7.
- (32) Toh, K. C.; Stojković, E. A.; Rupenyan, A. B.; van Stokkum, I. H. M.; Salumbides, M.; Groot, M.-L.; Moffat, K.; Kennis, J. T. M. Primary Reactions of Bacteriophytochrome Observed with Ultrafast Mid-Infrared Spectroscopy. *J. Phys. Chem. A* **2011**, *115* (16), 3778–3786.
- (33) Suzuki, H.; Okajima, K.; Ikeuchi, M.; Noguchi, T. LOV-Like Flavin-Cys Adduct Formation by Introducing a Cys Residue in the BLUF Domain of TePixD. *J. Am. Chem. Soc.* **2008**, *130* (39), 12884–12885.
- (34) Gauden, M.; van Stokkum, I. H. M.; Key, J. M.; Lührs, D. Ch.; van Grondelle, R.; Hegemann, P.; Kennis, J. T. M. Hydrogen-Bond Switching through a Radical Pair Mechanism in a Flavin-Binding Photoreceptor. *Proc. Natl. Acad. Sci. U. S. A.* **2006**, *103* (29), 10895–10900.
- (35) Holzer, W.; Penzkofer, A.; Hegemann, P. Absorption and Emission Spectroscopic Characterisation of the LOV2-His Domain of Phot from *Chlamydomonas Reinhardtii*. *Chem. Phys.* **2005**, *308* (1–2), 79–91.
- (36) Manathunga, M.; Yang, X.; Olivucci, M. Electronic State Mixing Controls the Photoreactivity of a Rhodopsin with All-Trans Chromophore Analogues. *J. Phys. Chem. Lett.* **2018**, *9* (21), 6350–6355.
- (37) Manathunga, M.; Yang, X.; Orozco-Gonzalez, Y.; Olivucci, M. Impact of Electronic State Mixing on the Photoisomerization Time Scale of the Retinal Chromophore. *J. Phys. Chem. Lett.* **2017**, *8* (20), 5222–5227.
- (38) Zhang, J.; Singh, P.; Engel, D.; Fingerhut, B. P.; Broser, M.; Hegemann, P.; Elsaesser, T. Ultrafast Terahertz Stark Spectroscopy Reveals the Excited-State Dipole Moments of Retinal in Bacteriorhodopsin. *Proc. Natl. Acad. Sci. U. S. A.* **2024**, *121* (26), 1–7.
- (39) Lin, C. Y.; Boxer, S. G. Mechanism of Color and Photoacidity Tuning for the Protonated Green Fluorescent Protein Chromophore. *J. Am. Chem. Soc.* **2020**, *142* (25), 11032–11041.
- (40) Bührke, D.; Hildebrandt, P. Probing Structure and Reaction Dynamics of Proteins Using Time-Resolved Resonance Raman Spectroscopy. *Chem. Rev.* **2020**, *120* (7), 3577–3630.
- (41) Myers, A. B. Relating Absorption, Emission, and Resonance Raman Spectra with Electron Transfer Rates in Photoinduced Charge Transfer Systems: Promises and Pitfalls. *Chem. Phys.* **1994**, *180* (2–3), 215–230.
- (42) Myers, A. B. Resonance Raman Intensities and Charge-Transfer Reorganization Energies. *Chem. Rev.* **1996**, *96* (3), 911–926.
- (43) Myers, A. B. Resonance Raman Intensity Analysis of Excited-State Dynamics. *Acc. Chem. Res.* **1997**, *30* (12), 519–527.
- (44) Heller, E. J.; Sundberg, R. L.; Tannor, D. Simple Aspects of Raman Scattering. *J. Phys. Chem.* **1982**, *86* (10), 1822–1833.
- (45) Lee, S.-Y.; Heller, E. J. Time-Dependent Theory of Raman Scattering. *J. Chem. Phys.* **1979**, *71* (12), 4777–4788.
- (46) Shim, S.; Stuart, C. M.; Mathies, R. A. Resonance Raman Cross-Sections and Vibronic Analysis of Rhodamine 6G from Broadband Stimulated Raman Spectroscopy. *ChemPhysChem* **2008**, *9* (5), 697–699.
- (47) Fumero, G.; Schnedermann, C.; Batignani, G.; Wende, T.; Liebel, M.; Bassolino, G.; Ferrante, C.; Mukamel, S.; Kukura, P.; Scopigno, T. Two-Dimensional Impulsively Stimulated Resonant Raman Spectroscopy of Molecular Excited States. *Phys. Rev. X* **2020**, *10* (1), 011051.
- (48) Weigel, A.; Dobryakov, A.; Klaumünzer, B.; Sajadi, M.; Saalfrank, P.; Ernsting, N. P. Femtosecond Stimulated Raman Spectroscopy of Flavin after Optical Excitation. *J. Phys. Chem. B* **2011**, *115* (13), 3656–3680.
- (49) Andrikopoulos, P. C.; Liu, Y.; Picchiotti, A.; Lenngren, N.; Kloz, M.; Chaudhari, A. S.; Precek, M.; Rebarz, M.; Andreasson, J.; Hajdu, J.; Schneider, B.; Fuertes, G. Femtosecond-to-Nanosecond Dynamics of Flavin Mononucleotide Monitored by Stimulated Raman Spectroscopy and Simulations. *Phys. Chem. Chem. Phys.* **2020**, *22* (12), 6538–6552.
- (50) Iuliano, J. N.; Hall, C. R.; Green, D.; Jones, G. A.; Lukacs, A.; Illarionov, B.; Bacher, A.; Fischer, M.; French, J. B.; Tonge, P. J.; Meech, S. R. Excited State Vibrations of Isotopically Labeled FMN Free and Bound to a Light–Oxygen–Voltage (LOV) Protein. *J. Phys. Chem. B* **2020**, *124* (33), 7152–7165.
- (51) Hontani, Y.; Mehlhorn, J.; Domratcheva, T.; Beck, S.; Kloz, M.; Hegemann, P.; Mathes, T.; Kennis, J. T. M. Spectroscopic and Computational Observation of Glutamine Tautomerization in the Blue Light Sensing Using Flavin Domain Photoreaction. *J. Am. Chem. Soc.* **2023**, *145* (2), 1040–1052.
- (52) Liu, Y.; Chaudhari, A. S.; Chatterjee, A.; Andrikopoulos, P. C.; Picchiotti, A.; Rebarz, M.; Kloz, M.; Lorenz-Fonfria, V. A.; Schneider, B.; Fuertes, G. Sub-Millisecond Photoinduced Dynamics of Free and EL222-Bound FMN by Stimulated Raman and Visible Absorption Spectroscopies. *Biomolecules* **2023**, *13* (1), 161–172.
- (53) Kloz, M.; Weissenborn, J.; Polívka, T.; Frank, H. A.; Kennis, J. T. M. Spectral Watermarking in Femtosecond Stimulated Raman Spectroscopy: Resolving the Nature of the Carotenoid S\* State. *Phys. Chem. Chem. Phys.* **2016**, *18* (21), 14619–14628.
- (54) Schelvis, J. P. M.; Ramsey, M.; Sokolova, O.; Tavares, C.; Cecala, C.; Connell, K.; Wagner, S.; Gindt, Y. M. Resonance Raman and UV–Vis Spectroscopic Characterization of FADH<sup>•</sup> in the Complex of Photolyase with UV-Damaged DNA. *J. Phys. Chem. B* **2003**, *107* (44), 12352–12362.
- (55) Snellenburg, J. J.; Laptinok, S. P.; Seger, R.; Mullen, K. M.; Stokkum, I. H. M. v. Glotaran: A Java-Based Graphical User Interface for the R Package TIMP. *J. Stat Softw* **2012**, *49* (3), 1–22.
- (56) Losi, A.; Kottke, T.; Hegemann, P. Recording of Blue Light-Induced Energy and Volume Changes within the Wild-Type and Mutated Phot-LOV1 Domain from *Chlamydomonas Reinhardtii*. *Biophys. J.* **2004**, *86* (2), 1051–1060.
- (57) Schüttrigkeit, T. A.; Kompa, C. K.; Salomon, M.; Rüdiger, W.; Michel-Beyerle, M. E. Primary Photophysics of the FMN Binding LOV2 Domain of the Plant Blue Light Receptor Phototropin of *Avena Sativa*. *Chem. Phys.* **2003**, *294* (3), 501–508.

- (58) Losi, A.; Polverini, E.; Quest, B.; Gärtner, W. First Evidence for Phototropin-Related Blue-Light Receptors in Prokaryotes. *Biophys. J.* **2002**, *82* (5), 2627–2634.
- (59) Green, D.; Roy, P.; Hall, C. R.; Iuliano, J. N.; Jones, G. A.; Lukacs, A.; Tonge, P. J.; Meech, S. R. Excited State Resonance Raman of Flavin Mononucleotide: Comparison of Theory and Experiment. *J. Phys. Chem. A* **2021**, *125* (28), 6171–6179.
- (60) Wei, L.; Min, W. Electronic Preresonance Stimulated Raman Scattering Microscopy. *J. Phys. Chem. Lett.* **2018**, *9* (15), 4294–4301.
- (61) Inagaki, F.; Tasumi, M.; Miyazawa, T. Excitation Profile of the Resonance Raman Effect of  $\beta$ -Carotene. *J. Mol. Spectrosc.* **1974**, *50* (1–3), 286–303.
- (62) Blazej, D. C.; Peticolas, W. L. Ultraviolet Resonant Raman Spectroscopy of Nucleic Acid Components. *Proc. Natl. Acad. Sci. U. S. A.* **1977**, *74* (7), 2639–2643.
- (63) Peticolas, W. L.; Blazej, D. C. Estimation of the Distortion of the Geometry of Nucleic-Acid Bases in the Excited Electronic State from the Ultraviolet Resonance Raman Intensity of Certain Normal Modes. *Chem. Phys. Lett.* **1979**, *63* (3), 604–608.
- (64) Blazej, D. C.; Peticolas, W. L. Ultraviolet Resonance Raman Excitation Profiles of Pyrimidine Nucleotides. *J. Chem. Phys.* **1980**, *72* (5), 3134–3142.
- (65) Tannor, D. J.; Heller, E. J. Polyatomic Raman Scattering for General Harmonic Potentials. *J. Chem. Phys.* **1982**, *77* (1), 202–218.
- (66) Gill, D.; Heyde, M. E.; Rimai, L. Raman Spectrum of the 11-Cis Isomer of Retinaldehyde. *J. Am. Chem. Soc.* **1971**, *93* (23), 6288–6289.
- (67) Heyde, M. E.; Gill, D.; Kilponen, R. G.; Rimai, L. Raman Spectra of Schiff Bases of Retinal (Models of Visual Photoreceptors). *J. Am. Chem. Soc.* **1971**, *93* (25), 6776–6780.
- (68) Spiro, T. G.; Stein, P. Resonance Effects in Vibrational Scattering from Complex Molecules. *Annu. Rev. Phys. Chem.* **1977**, *28* (1), 501–521.
- (69) Farag, M. H.; Jansen, T. L. C.; Knoester, J. Probing the Interstate Coupling near a Conical Intersection by Optical Spectroscopy. *J. Phys. Chem. Lett.* **2016**, *7* (17), 3328–3334.
- (70) Pupeza, I.; Huber, M.; Trubetskoy, M.; Schweinberger, W.; Hussain, S. A.; Hofer, C.; Fritsch, K.; Poetzlberger, M.; Vamos, L.; Fill, E.; Amotchkina, T.; Kepesidis, K. V.; Apolonski, A.; Karpowicz, N.; Pervak, V.; Pronin, O.; Fleischmann, F.; Azzeer, A.; Zigman, M.; Krausz, F. Field-Resolved Infrared Spectroscopy of Biological Systems. *Nature* **2020**, *577* (7788), 52–59.
- (71) Anderson, P. W. More Is Different. *Science* **1972**, *177* (4047), 393–396.
- (72) Möglich, A.; Moffat, K. Structural Basis for Light-Dependent Signaling in the Dimeric LOV Domain of the Photosensor YtvA. *J. Mol. Biol.* **2007**, *373* (1), 112–126.
- (73) Halavaty, A. S.; Moffat, K. N- and C-Terminal Flanking Regions Modulate Light-Induced Signal Transduction in the LOV2 Domain of the Blue Light Sensor Phototropin 1 from *Avena Sativa*. *Biochemistry* **2007**, *46* (49), 14001–14009.
- (74) Guntas, G.; Hallett, R. A.; Zimmerman, S. P.; Williams, T.; Yumerefendi, H.; Bear, J. E.; Kuhlman, B. Engineering an Improved Light-Induced Dimer (ILID) for Controlling the Localization and Activity of Signaling Proteins. *Proc. Natl. Acad. Sci. U. S. A.* **2015**, *112* (1), 112–117.
- (75) Christie, J. M.; Hitomi, K.; Arvai, A. S.; Hartfield, K. A.; Mettlen, M.; Pratt, A. J.; Tainer, J. A.; Getzoff, E. D. Structural Tuning of the Fluorescent Protein ILOV for Improved Photostability. *J. Biol. Chem.* **2012**, *287* (26), 22295–22304.
- (76) Fedorov, R.; Schlichting, I.; Hartmann, E.; Domratheva, T.; Fuhrmann, M.; Hegemann, P. Crystal Structures and Molecular Mechanism of a Light-Induced Signaling Switch: The Phot-LOV1 Domain from *Chlamydomonas Reinhardtii*. *Biophys. J.* **2003**, *84* (4), 2474–2482.
- (77) Conrad, K. S.; Bilwes, A. M.; Crane, B. R. Light-Induced Subunit Dissociation by a Light–Oxygen–Voltage Domain Photoreceptor from *Rhodospira rubra*. *Biochemistry* **2013**, *52* (2), 378–391.
- (78) Lamb, J. S.; Zoltowski, B. D.; Pabit, S. A.; Li, L.; Crane, B. R.; Pollack, L. Illuminating Solution Responses of a LOV Domain Protein with Photocoupled Small-Angle X-Ray Scattering. *J. Mol. Biol.* **2009**, *393* (4), 909–919.
- (79) Weber, A. M.; Kaiser, J.; Ziegler, T.; Pils, S.; Renzl, C.; Sixt, L.; Pietruschka, G.; Moniot, S.; Kakoti, A.; Juraschitz, M.; Schrottke, S.; Lledo Bryant, L.; Steegborn, C.; Bittl, R.; Mayer, G.; Möglich, A. A Blue Light Receptor That Mediates RNA Binding and Translational Regulation. *Nat. Chem. Biol.* **2019**, *15* (11), 1085–1092.
- (80) Hasegawa, J. ya; Bureekaew, S.; Nakatsuji, H. SAC-CI Theoretical Study on the Excited States of Lumiflavin: Structure, Excitation Spectrum, and Solvation Effect. *J. Photochem. Photobiol. A Chem.* **2007**, *189* (2–3), 205–210.